Electronic Supplementary Information (ESI) for Energy & Environmental Science.
This journal is © The Royal Society of Chemistry 2015

Supplementary Information for 17.6% stabilized efficiency in low-temperature processed planar perovskite solar cells

Chen Tao,[a] Stefanie Neutzner,[ab] Letizia Colella,[cd] Sergio Marras,[e] Ajay Ram Srimath Kandada,[a] Marina Gandini,[ab] Michele De Bastiani,[a] Giuseppina Pace,[a] Liberato Manna,[e] Mario Caironi,[a] Chiara Bertarelli[ac] and Annamaria Petrozza*[a]

[a]Center for Nano Science and Technology @Polimi, Istituto Italiano di Tecnologia, via Giovanni Pascoli 70/3, 20133, Milan, Italy

[b]Dipartimento di Fisica, Politecnico di Milano, Piazza L. da Vinci, 32, 20133 Milano, Italy

[c]Dipartimento di Chimica, Materiali e Ing. Chimica "G. Natta", Politecnico di Milano, Piazza L. Da Vinci 32, 20133 Milano, Italy

[d]NAF, Osservatorio Astronomico di Brera, via Bianchi 46, 23807 Merate, Italy

[e]Department of Nanochemistry, Istituto Italiano di Tecnologia, via Morego, 30, 16163 Genova, Italy

1. Experimental details

TiO_x synthesis: TiO_x precursor was synthesized with a modified recipe reported in Ref. 1. The reaction was carried out in dried glassware and under argon atmosphere. Air- and water-sensitive compounds were transferred with hypodermic syringes. 2 mL of titanium (IV) *iso*propoxide (Aldrich, 99.999%) was mixed with 10 mL of 2-methoxylethanol (Aldrich, 99.9+%) and 1 mL of ethanolamine (Aldrich, 99+%) in a three-necked flask equipped with a condenser and a thermometer. Then, the mixed solution was stirred at 80 ˚C for 2 h in silicon-oil bath, then heated to 120 ˚C for 1 h. The two-step heating (80 and 120 ˚C) was then repeated. It should be noted that all the chemical compounds were kept in the flask all the time under inert atmosphere. The TiO_x precursor solution for device fabrication was diluted in anhydrous 2-propanol with 1:41 (*v:v*).

Methyammonium iodide (CH_3NH_3I) precursor synthesis: Methylamine (CH_3NH_2) solution (33 wt% in anhydrous ethanol) was reacted with hydriodic acid (HI, 57 wt% in water) in ethanol at room temperature. Typical quantities of reactants are: 96 mL of methylamine solution, 40 mL of hydriodic acid, and 400 mL of ethanol. Solvent removal by rotary evaporator afforded CH_3NH_3I as a white crystalline powder, which is then washed twice in diethyl ether and dried in a fume hood overnight.

Device fabrication and characterization: Prior to the device fabrication, FTO-coated glass sheets were etched with zinc powder and HCl (2 M) to obtain the required electrode pattern. The substrates were then sonicated in sequence with detergent (alconox), distilled water, acetone and 2-propanol for 5 min, respectively. The substrates were then blown dry with N_2 and finally treated with oxygen plasma for 10 min to remove the last traces of organic residues.

As to TiO_2-based devices, a TiO_2 precursor was spin-coated at 2000 rpm for 40 s and then sintered at 500 °C following Ref. Ball, J. et al in *Energy Environ. Sci.* **6,** 1739 (2013): 35 uL of 2 M HCl was added dropwise under

vigorous stirring to a titanium isopropoxide solution in 2-propanol (369 uL titanium isopropoxide in 2.53 mL of 2-propanol). In the case of TiO_X/60-PCBM devices, diluted TiO_X was spin-coated onto FTO at 4000 rpm for 30 s. Then the samples were transferred into a N_2-filled glove box for 60-PCBM deposition. 10 mg mL^{-1} 60-PCBM dissolved in anhydrous chlorobenzene was spin-coated on top of TiO_X at 4000 rpm for 30 s followed by the samples being dried on a hotplate at 70 ˚C for 10 min.

Subsequently both TiO_2 and TiO_X/60-PCBM substrates were transferred into an evaporation chamber for PbI_2 sublimation followed by MAI spin-coating. Then the samples were annealed at 100 ºC for 80 min. The hole extracting material was then spin-coated at 4000 rpm for 30 s. The spin-coating formation was prepared by dissolving 72.3 mg (2,2',7,7'-tetrakis(*N,N*-di-*p*-methoxyphenylamine)-9,9-spirobifluorene) (spiro-MeOTAD), 28.8 uL 4-*tert*-butylpyridine, 17.5 uL of a stock solution of 520 mg mL^{-1} lithium bis(trifluoromethylsulphonyl)imide in acetonitrile in 1 mL anhydrous chlorobenzene. Finally, 70 nm gold was thermally evaporated through a shadow mask to create devices with total area of ca. 0.08 cm^2.

The current density-voltage (*J-V*) characteristics were measured with a computer-controlled Keithley 2400 source meter in air without any device encapsulation. The simulated Air Mass 1.5 Global (AM 1.5G) irradiance was provided with a class AAA Newport solar simulator. The light intensity was calibrated with a silicon reference cell with a spectral mismatch factor of 0.99. For the *J-V* measurement, the voltage step and delay time were 20 mV and 10 ms, respectively. Particularly longer delay time were specified in the context. The forward scan started from 0 V (the short circuit condition) to 1.2 V, while reverse scan from 1.2 V to 0 V. It should be noted that in our case that the forward and reverse scan are not a cycle one. The pre-condition for both scans was the same, that is, just with 10 s light exposure. The stabilized current density and power output were recorded close to the maximum power point, which was at 0.917 V in Fig. 3 (such voltage has been extracted by the *J-V* characteristic in Fig 2.b). The delay time is 10 ms. The EQE was measured with a home-built setup. EQE spectra were recorded using the monochromated (Bentham) output from a tungsten halogen lamp calibrated with a Newport UV-181 photodiode; phase-sensitive detection with a lock-in amplifier was used to increase the signal-to-noise ratio. XRD patterns were recorded with a Rigaku SmartLab X-Ray diffractometer equipped with a 9 kW Cu$K\alpha$ rotating anode, operating at 40 kV and 150 mA. A Göbel mirror was used to convert the divergent X-ray beam into a parallel beam and to suppress the Cu $K\beta$ radiation (1.392 Å). The diffraction patterns were collected at room temperature over an angular range $2\theta = 10° - 60°$, with a step size of 0.02° in a symmetric $2\theta/\omega$ scan reflection mode. The cross sections were realized and acquired using a FEI Nova 600 NanoLab DualBeam SEM/FIB. A precisely focused Ga+ ion beam was obtained operating at 24 pA and 30 kV, while SEM imaging was performed at 5 kV using an in-lens secondary electron detector.

Fs-transient absorption spectroscopy: For the fs-TA measurements, the output of a Coherent Micra Ti:Sapphire oscillator in conjunction with a Coherent RegA 9040 amplifier (800 nm, 40 fs pulse duration and 250 kHz repetition rate) was split into two parts. One part of the laser output pumped a Coherent collinear optical parametric amplifier to generate pump pulses at 650 nm. The other part was used as probe after white light generation in a sapphire plate. The delay between the pump and the probe pulses was controlled by a motorized delay-stage and the signal was detected using a customized CCD-camera with electronic shutter. For the measurements, the pump beam of 1.6 nJ excitation power was focused on approximately 1 mm^2 device area. All measurements were carried out in vacuum, using a continuous flow static exchange gas cryostat (Oxford Instruments Optistat CF). For monitoring the current in short-circuit condition and applying a bias voltage, the devices were connected to an Agilent B2912A source/measure unit.

AFM Measurements: The surface topography of the films was measured with an Agilent 5500 Atomic Force Microscope operated in the Acoustic Mode.

Kelvin-Probe Measurements: The contact potential of samples have been extracted by performing Kelvin-Probe measurements with the Ambient Kelvin Probe instrument KP020 (KP Technologies), adopting a gold tip with 2 mm diameter. The absolute work-function values have been extracted with respect to a freshly exfoliated HOPG sample.

2. Results

sample	work function (eV)
FTO	4.98
FTO/TiO_X	4.61
FTO/TiO_X/60-PCBM	4.36

Table S1. Work function of different samples

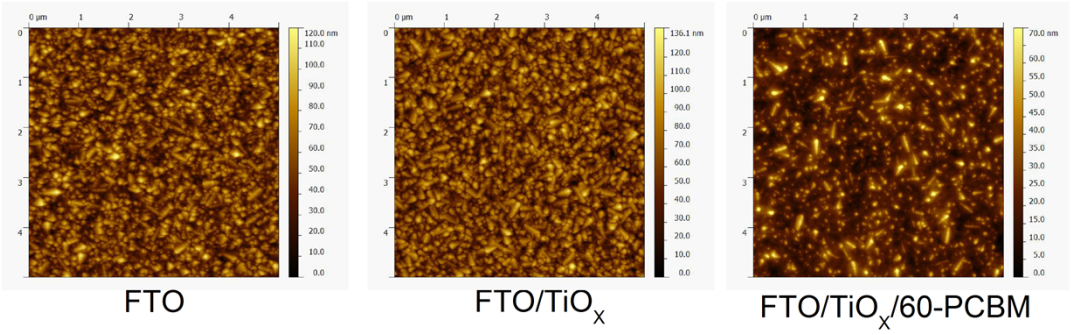

Fig S1

sample	**FTO**	**FTO/TiO_X**	**FTO/TiO_X/60-PCBM**
rms (nm)	**16**	**18**	**10**

Table S2

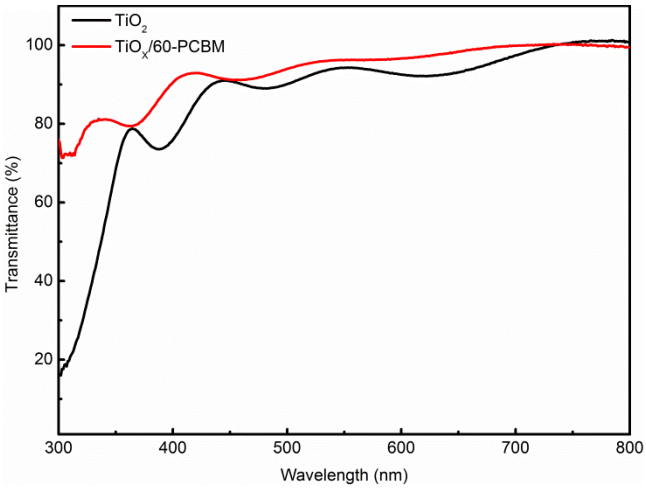

Fig. S2 Optical transmission spectra of eletron-extracting layers in the visible range that were performed using a spectrophotometer (Varian Cary 50 Scan).

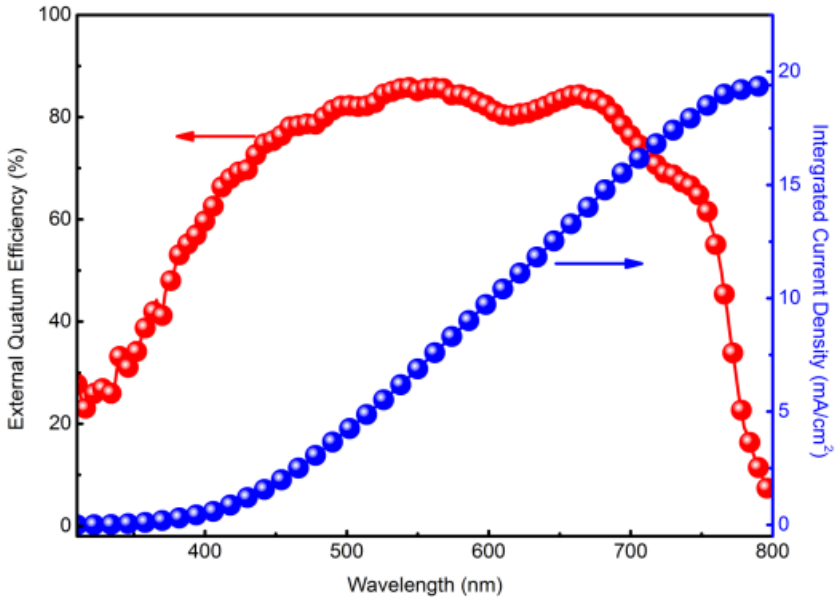

Fig. S3 EQE response spectrum of a typical TiOx/60-PCBM-based device.

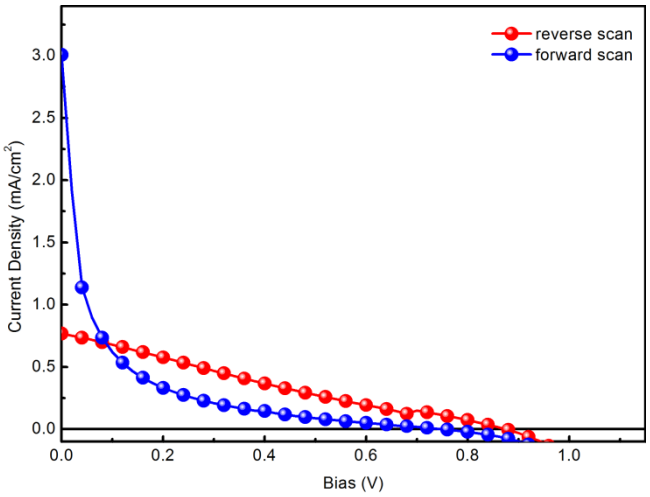

Fig. S4 *J-V* curves of a TiO_X-only device with the structure of FTO/TiO_X/$CH_3NH_3PbI_3$/spiro-MeOTAD/Au under 87.3 mW cm^{-2} white light illumination.

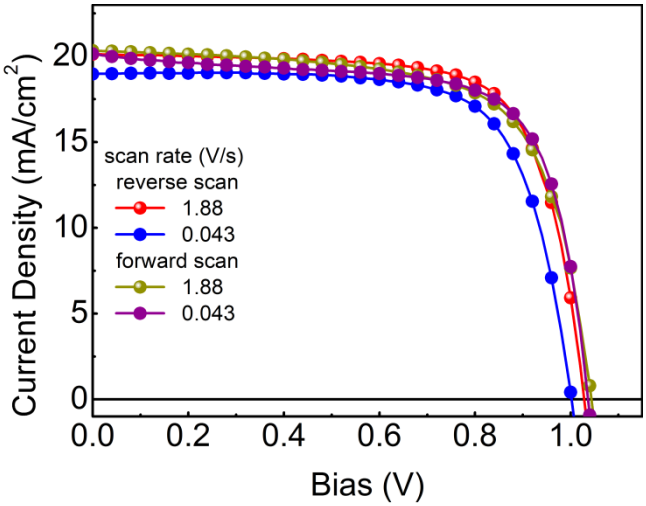

Fig. S5 *J-V* curves of a device with the structure of FTO/TiO_2/60-PCBM/$CH_3NH_3PbI_3$/spiro-MeOTAD/Au

device	scan rate (V s^{-1})		V_{OC} (V)	J_{SC} (mA cm^{-2})	FF (%)	PCE (%)
TiO_2/60-PCBM	reverse scan	1.88	1.03	20.1	72.4	15.0
		0.043	1.00	19.0	71.9	13.7
	forward scan	1.88	1.04	20.3	68.1	14.5
		0.043	1.04	20.1	70.9	14.7

Table 3

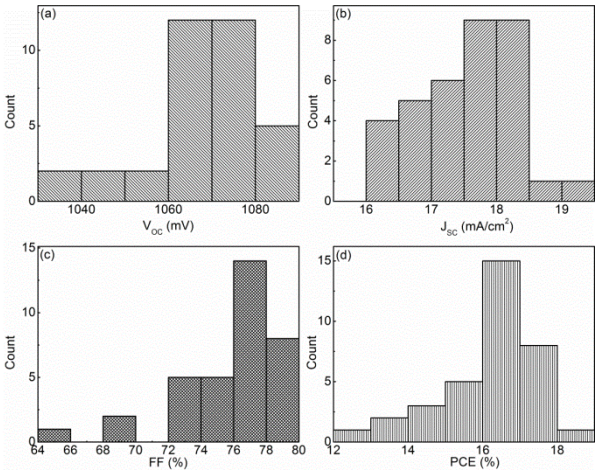

Fig. S6a Histograms of device performances measured under 87.3 mW cm^{-2} white light illumination for 38 individual devices with reverse scans.

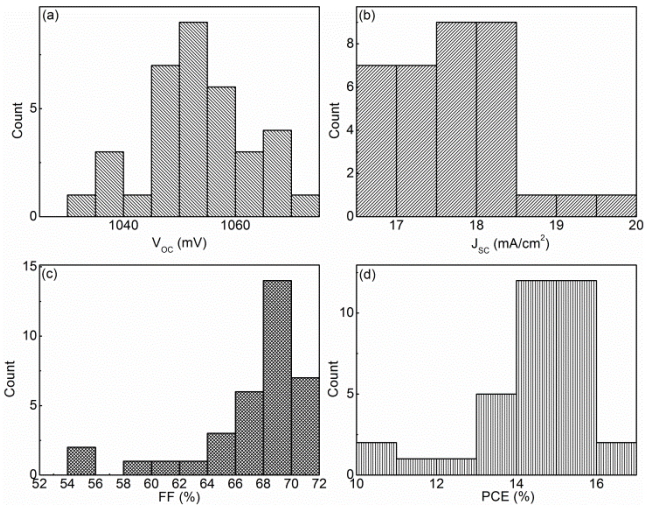

Fig. S6b Histograms of device performances measured under 87.3 mW cm^{-2} white light illumination for 38 individual devices with forward scans.

Though the statistic has been performed by testing the devices at an incident power slightly lower than 1 Sun (0.87 Sun), the results can be safely compared to those showed in the main manuscript as we found a linear dependence of the J_{SC} as a function of the incident power (see Fig. S7 below) and the PCE is measured as $Power_{out}/Power_{in}$, thus it is independent on the excitation density.

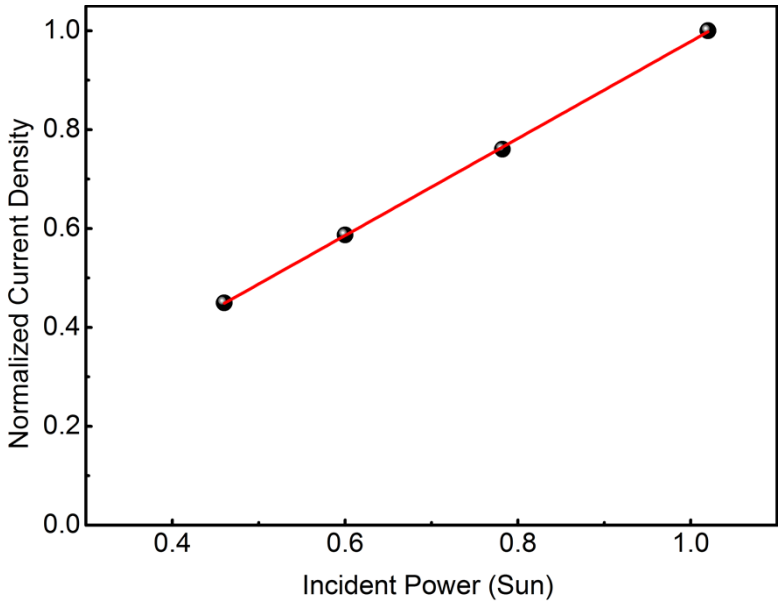

Fig. S7

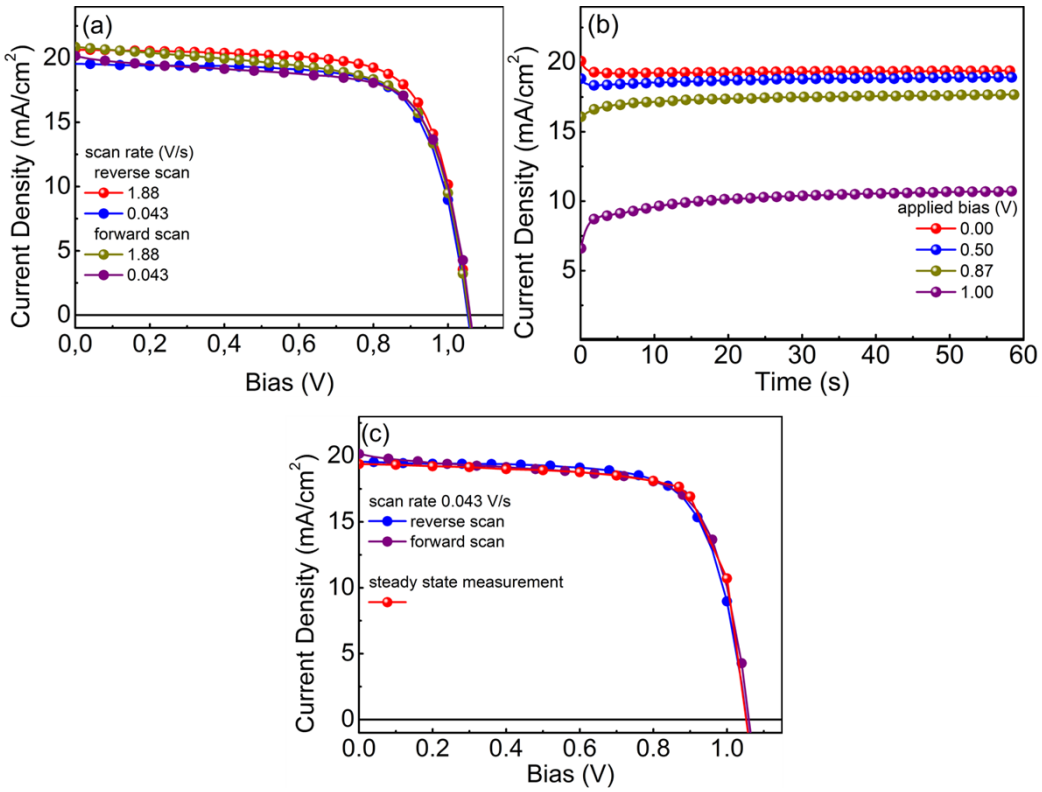

Fig. S8 (a) *J-V* characteristics of an aged (96 days in dark, N_2 atmosphere) device tested at different scan rates as in Fig. 2 of the manuscript. (b) stabilized current densities under four different representative applied biases. (c) *J-V* characteristics built by taking the plateau values of the photocurrent at different voltages. it is compared to the *J-V* characteristics taken at a scan rate of 0.043 V s^{-1} in (a). This demonstrates the reliability of freshly made devices shown in the main manuscript..

To provide a flavor of the device stability in Fig. S8, we compare the *J-V* characteristics of a fresh device (Fig. S9a) and of the same device tested 96 days later (Fig. S9b). The devices were exposed to air without any encapsulation during the tests and stored in nitrogen. In Table S4 the figure of merits are shown. Overall, the aging induces a loss in power conversion efficiency (PCE) of less than the 10%, mainly due to a loss in FF.

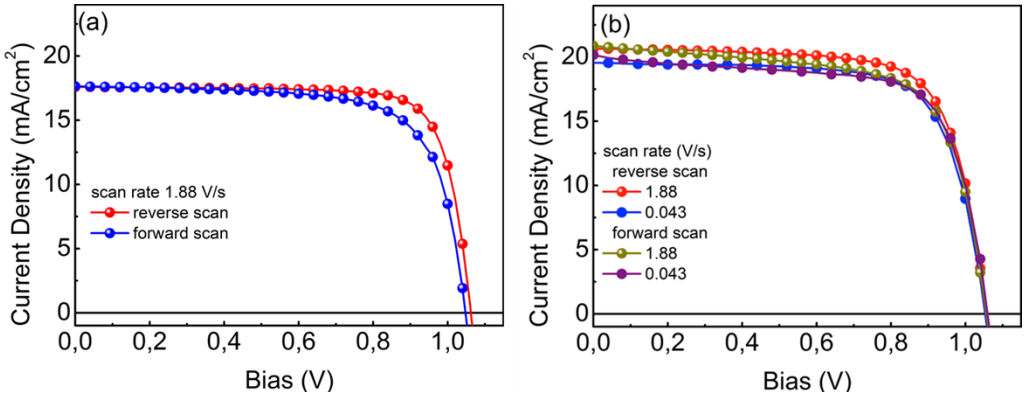

Fig. S9

device	scan rate (V s^{-1})		V_{OC} (V)	J_{SC} (mA cm^{-2})	FF (%)	PCE (%)
fresh	reverse scan 1.88		1.06	17.6	78.5	16.8
	forward scan 1.88		1.05	17.6	71.6	15.1
96-days-aged	reverse scan	1.88	1.06	20.7	72.6	15.8
		0.043	1.05	19.5	72.6	14.9
	forward scan	1.88	1.06	20.9	68.5	15.1
		0.043	1.06	20.1	70.6	15.0

Table S4

To be noted that the fresh device was measured under 0.873 Sun illumination while the aged devices have been tested under 1 sun. This explains why the J_{SC} is lower for the fresh that for the aged ones. However, by considering the simple ratio J_{SC}/P_{in} of the fresh and aged devices we find that it is linear ($\frac{17\ mA\ -2}{87\ mW-2} = 0.2; \frac{20.7\ mA-2}{100\ mW\ cm2} = 0.2$). It highlights that there is no drop in current density in the aged devices. Finally, as the PCE is calculated as the ratio between the incident and delivered power ($\eta = P_{out}/P_{in}$) the comparison remains valid.

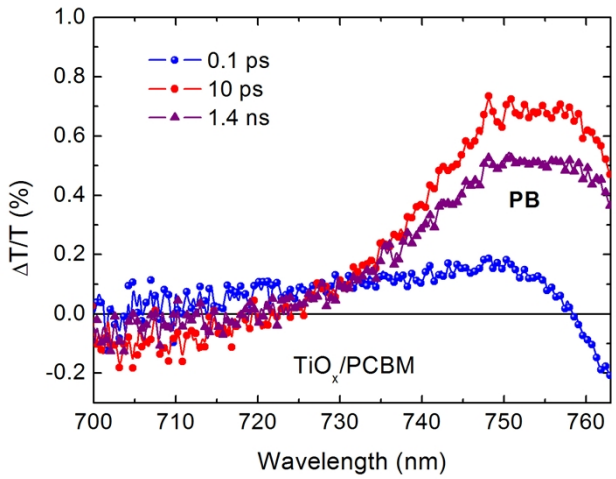

Fig. S10 TA spectral dynamics of the photo-excited perovskites in working devices under short-circuit condition at 100 fs, 10 ps and 1.4 ns delay time. The broad positive band seen at 100 fs delay is associated to the photo-bleaching of the material due to the presence of hot carriers[2] and the negative band at 765 nm has been assigned to band gap renormalization[3]. In a few picoseconds the PB band redshifts and peaks at around 750-755 nm due to carrier thermalization as seen in the spectrum at 10 ps.[2] The intensity of the PB band is proportional to the density of carriers present within the material and hence it is quenched in the nanoseconds timescale due to the extraction of the carriers within the device.

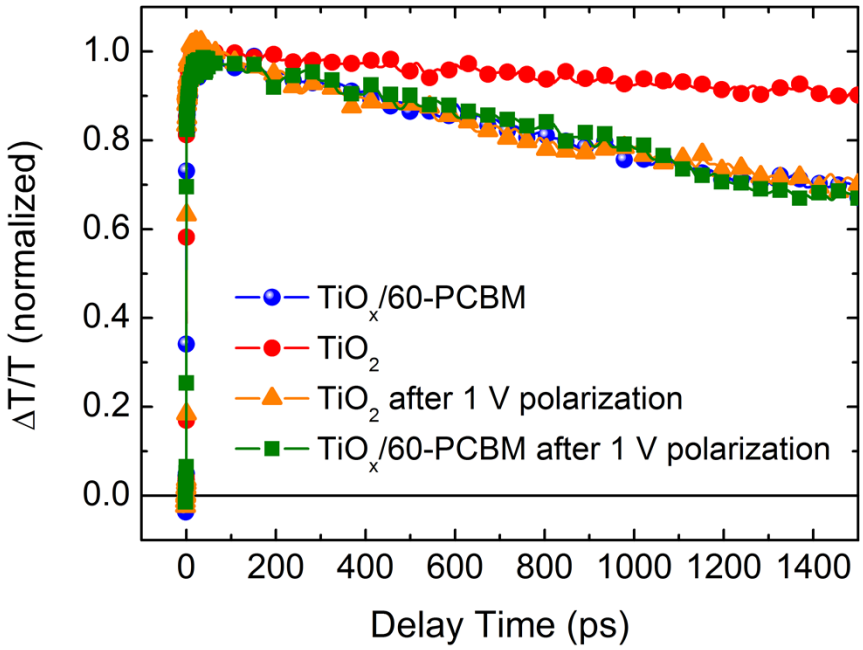

Fig. S11: The dynamics of the photo-bleaching bands for the photo-excited perovskites in working devices under short-circuit condition.

Reference:

1 J. Y. Kim, S. H. Kim, H.-H. Lee, K. Lee, W. Ma, X. Gong, and A. J. Heeger, *Adv. Mater.*, 2006, **18**, 572.

2 J. S. Manser, and P. V. Kamat, *Nat. Photonics*, 2014, **8,** 737.

3 F. Deschler, M. Price, S. Pathak, L. E. Klintberg, D.-D. Jarausch, R. Higler, S. Hüttner, T. Leijtens, S. D. Stranks, H. J. Snaith, M. Atatüre, R. T. Phillips, and R. H. Friend, *J. Phys. Chem. Lett.*, 2014, **5**, 1421.